Behavior of wire arc additively manufactured 316L austenitic stainless steel single shear bolted connections

Behavior of wire arc additively manufactured 316L austenitic stainless steel single shear bolted connections

Wenkang Zuo [a, b], Man-Tai Chen [a, b] *, Ou Zhao [c], Andi Su [d],

Si-Wei Liu [e], Fangda Xu [f], Yuner Huang[g], Bin Cheng [a, b]

[a] *State Key Laboratory of Ocean Engineering, Shanghai Jiao Tong University, Shanghai 200240, China*
[b] *Shanghai Key Laboratory for Digital Maintenance of Buildings and Infrastructure, Department of Civil Engineering, Shanghai Jiao Tong University, Shanghai 200240, China*
[c] *School of Civil and Environmental Engineering, Nanyang Technological University, Singapore*
[d] *Key Lab of Structures Dynamic Behaviour and Control of the Ministry of Education, Harbin Institute of Technology, Harbin, 150090, China*
[e] *Dept. of Civil and Environmental Engineering, The Hong Kong Polytechnic Univ., Hong Kong 999077, China.*
[f] *Rongsu Technology Ltd, Suzhou, China*
[g] *School of Engineering, University of Edinburgh, Edinburgh, Scotland, UK.*

Abstract: This paper aims to investigate the behavior of single shear bolted connections made of wire arc additively manufactured 316L austenitic stainless steel. A set of 44 wire arc additive manufacturing (WAAM) 316L austenitic stainless steel single shear bolted connections were included with consideration of various bolt positions, surface conditions and loading orientations respective to the printing layer direction. The geometric dimensions of the WAAM austenitic stainless steel plates were measured with the assistance of non-contact 3D laser scanning prior to tensile testing. Monotonic tensile tests were carried out to investigate the load-deformation responses, failure patterns and resistances determined by both the deformation and strength criteria of the single shear bolted connections. The effects of geometric and printing parameters on the single shear bolted connections were analyzed. Due to the absence of codified design provisions for WAAM austenitic stainless steel bolted connections, the suitability of the existing design rules originally developed for traditionally manufactured carbon steel and stainless steel bolted connections was examined. Design resistances calculated by the Eurocode 3 (prEN 1993-1-8 and prEN 1993-1-4), the American Specification (ANSI/AISC 370-21) as well as the prevalent design recommendations proposed in existing literature were compared with the obtained experimental results. It is shown that the abovementioned design methods offer conservative predictions for the resistances of WAAM 316L austenitic stainless steel single shear bolted connections. Further study is needed to improve the accuracy of design resistance predictions.

Keywords: wire arc additive manufacturing (WAAM), metallic 3D printing, single shear, bolted connections, austenitic stainless steel.

* Corresponding author.
E-mail address: mantai.chen@sjtu.edu.cn (Man-Tai Chen).

1. Introduction

Recent advancements in the steel manufacturing industry, have led to heightened expectations for the design of steel structures, thereby necessitating the development and application of high-performance standards. This surge in demand has prompted the structural design and construction sectors to actively pursue innovative solutions aimed at enhancing structural performance [1-5], optimizing design efficiency [6-11], and streamlining construction processes [12]. Across the globe, endeavors encompassing the development and exploration of high-performance materials [13-16], advanced structural configurations [17-23] and inventive construction methodologies [24-26] have been actively pursued and investigated. Metallic additive manufacturing (AM) stands as a groundbreaking technology pivotal for industrial progress due to its ability to offer design flexibility, shorter production times and minimal environmental impact [27, 28]. Notably, the construction industry has increasingly expressed interest in utilizing metallic components made through AM for structural purposes. Additionally, researchers worldwide are placing greater emphasis on conducting extensive investigations and studies in this domain. Wire arc additive manufacturing (WAAM) is a type of 3D printing or additive manufacturing technique that uses an electric arc as the heat source to deposit metal wire material layer by layer [29, 30]. Wire arc additive manufacturing technology presents substantial potential in constructing large-scale steel structures with complex configurations, due to its relatively high deposition rate, low cost and less limitation on building size [31, 32].

Bolted connections stand as the predominant load transferring method employed in steel construction, which are integral in providing flexibility for assembly/disassembly as well as assuring the structural integrity and longevity. Abundant investigations have been conducted on bolted connections of traditional steel members (e.g., normal strength [33, 34] and high strength carbon steel [35-37], stainless steel [38-41]). The corresponding design methods have been proposed accordingly by researchers and codified in the design guidelines. Gaining essential insights into the structures created through wire arc additive manufacturing and advancing the utilization of WAAM technology in structural applications necessitate a thorough grasp of the structural behavior of WAAM steel

connections. Recently, Guo et al. [42, 43], Ye *et al.* [44] and Liu *et al.* [45] have reported a series of experimental investigations on WAAM carbon steel single-lap and double-lap shear bolted connections manufactured by feedstock wire of AWS ER70S-6. The test results revealed that the loading direction respective to printing direction of WAAM steel specimens influenced the failure modes of connections with identical geometric parameters and bolt hole locations. Comparing to the specimens with the loading direction perpendicular to printing direction, the counterparts with the loading direction parallel to printing direction were sometimes more inclined to exhibit lower resistances to end-splitting since the fracture lines propagated along the interface of adjacent print layers. However, the behavior of WAAM austenitic stainless steel bolted connections is scarce. It was reported that the material anisotropy of WAAM stainless steel is usually more prominent than that of WAAM carbon steel [46-49]. Furthermore, WAAM austenitic stainless steel bolted connection susceptible to bearing failure is expected to exhibit large bolt hole deformation due to its significantly greater material ductility compared to WAAM carbon steel. This could potentially require the inclusion of bolt hole deformation when formulating bearing strength design rules.

To address the identified research gap, this paper presents an experimental investigation into the structural behavior of WAAM 316L austenitic stainless steel shear bolted connections. A total of 44 WAAM austenitic stainless steel single shear bolted connections were fabricated and tested. The fabrication process, geometry measurement, and material property determination of the connection specimens are detailed. The setup and procedures for the single shear bolted connection tests are outlined. Key test results, including load-deformation performance, resistance and typical failure patterns, are reported. The effects of bolt position and test orientation of WAAM austenitic stainless steel plate on the connection behavior are discussed. To evaluate the applicability of current design rules for WAAM austenitic stainless steel single shear bolted connections, the connection resistances calculated by the Eurocode 3 (prEN 1993-1-8 [50] and prEN 1993-1-4 [51]), the American Specification ANSI/AISC 370-21 [52] as well as the prevalent design recommendations [34, 42] are compared against the experimental results.

2. Specimen details

2.1. Fabrication process of specimens

The Fronius TPS 400i metal inert gas system, paired with a six-axis KUKA robotic arm was utilized in this study, as shown in Fig. 1 (a). Feedstock wire of ER316L austenitic stainless steel with a diameter of 1.2 mm was employed to fabricate the flat oval shaped tubes through WAAM. The chemical composition of the ER316L austenitic stainless steel wire provided by the manufacturer is presented in Table 1. The reported tensile strength of the austenitic stainless steel wire in the mill certificate is 568 MPa and the elongation after fracture is 39%. The WAAM process utilized Cold Metal Transfer (CMT) technology, chosen for its minimized heat input, high deposition rate and deposition without spattering. The manufacturing parameters, such as wire feeding rate (5 m/min), travel speed (0.6 m/min), interlayer temperature (200°C), arc voltage (19.6 V) and current (144 A), were designed and properly controlled during the WAAM process. Afterwards, the WAAM austenitic stainless steel plates, forming the connection specimens, were obtained by wire cutting from the flat segments of flat oval shaped tubes with the aid of coolant, in order to minimize the extra heat introduced during the cutting process (Fig. 1 (b)). For machined connection specimens, the surfaces of WAAM austenitic stainless steel plates underwent additional milling to achieve smooth and uniform surfaces. The bolt holes were fabricated by drilling.

2.2. Design of single shear bolted connections

All WAAM austenitic stainless steel bolted connection specimens in this study featured a one-bolt configuration. Two distinct surface conditions were considered, namely unmachined (UM) ones with original geometric undulations and machined (M) ones with smooth surfaces, as shown in Fig. 2. It was reported in previous studies that WAAM austenitic stainless steel possessed significant anisotropy in material properties [49, 53]. Therefore, five different test orientations (θ=0°, 30°, 45°,

60°, 90°) were included to study the effect of material anisotropy on the connection behavior, where θ is the angle between the printing direction and the loading direction of connection (see Fig. 2). In contrast to double-lap shear connections where curl-bearing failure is not a concern, the occurrence of end curling could have a significant impact on the structural performance of the single-lap shear connections, particularly for connections with smaller plate thickness [54, 55], although curling was usually not the direct cause of failure [42]. To consider such effect, the designed thickness of machined specimens was taken as 3.5 mm in this study. The position of bolt hole was determined by the end distance (e_1 and e_1') and edge distance (e_2 and e_2') defined in Fig. 3. The values of end and edge distances were properly designed to encompass typical failure patterns, including net section fracture, shear-out, localized tearing and curl-bearing failures. The nominal e_1'/d_0 varied from 1.0 to 4.0 and e_2'/d_0 varied from 0.8 to 3.0, and d_0 is the diameter of bolt hole. A total of 44 WAAM austenitic stainless steel single shear bolted connections, including three repeated specimens, were designed.

The WAAM austenitic stainless steel single shear bolted connection specimens are labelled according to the following conventions. The letter(s) before the first hyphen 'UM' or 'M' indicates unmachined or machined specimen, respectively, followed by the value of test orientation (θ). Then the position of bolt hole is specified by the nominal clear end and edge distances ratios of e_1'/d_0 and e_2'/d_0 with the corresponding values shown before and after the last hyphen, respectively. The last letter 'R' if any represents a repeat test. For instance, M-90-1.5-3.0R refers to a repeated WAAM austenitic stainless steel single shear bolted connection with machined flat and smooth surfaces, the applied load perpendicular to the printing direction, the values of e_1'/d_0 and e_2'/d_0 being 1.5 and 3.0, respectively.

2.3. Geometric measurements

The latest seven-axis FARO ScanARM depicted in Fig. 4 (a), a non-contact 3D laser scanning device endowed with arm-like joints enabling free movement and empowered by a high-precision laser line probe, was used to determine the geometries of unmachined WAAM austenitic stainless

steel sheets possessing noticeable surface undulations prior to coupon tests and bolt connection tests. The obtained point cloud data was processed using Geomagic Design X software [56] to create CAD model and then imported into Rhino [57] for further analysis (Fig. 4 (b)). Geometric analysis was performed using Grasshopper [58], a visual programming platform for parametric design embedded in Rhino [57]. The parametric geometric analysis program proposed by Chen's Group [48, 49, 59] was adopted to automatically generate a myriad of virtual points delineating the intricate external surface pattern. This facilitated the determination of specimen geometries such as specimen thickness at arbitrary position.

Dense point cloud with a uniform interval of 0.05 mm was used to replicate the geometric features of each unmilled specimen. Schematic view of cloud point generation for geometric analysis in Rhino 3D is depicted in Fig. 5 (a). The thickness values of the unmachined specimens provided in Table 2 were determined by averaging the measurements obtained from 3D scanning according to the method detailed in literature [59]. The cumulative distribution and relative frequency histograms of specimen thickness for a typical unmilled specimen UM-90-1.5-3.0 are depicted in Fig. 5 (b). The findings indicated that the thickness distribution of WAAM austenitic stainless steel specimen generally follows a normal distribution. The mean thickness value was 6.61 mm, with the 5% and 95% fractile values of 6.38 mm (d_5) and 6.85 mm (d_{95}), respectively.

As for WAAM austenitic stainless steel specimens with machined flat and smooth surfaces, the geometric dimensions were manually measured via vernier calipers. The obtained geometric properties of WAAM austenitic stainless steel sheets for bolted connection specimens are summarized in Table 2, where b and t denote the width and thickness of the WAAM austenitic stainless steel sheets as defined in Fig. 3.

2.4. Material properties tests

The material properties of the WAAM 316L austenitic stainless steel specimens were obtained from a series of tensile coupon tests. Coupon specimens were extracted from the same batch of

WAAM austenitic stainless steel flat oval tube. To account for the material anisotropy, five different test orientations defined by the angle between the printing and the loading directions (θ=0°, 30°, 45°, 60°, 90°) were considered for machined coupons (labeled as M0, M30, M45, M60, M90, respectively). Meanwhile, the unmachined coupons with two typical test orientations of 0° and 90° (labeled as UM0 and UM90) were also included. The dimensions of coupons were designed in accordance with the ASTM-E8M [60]. The coupon tests were performed using a displacement-controlled testing scheme. A calibrated extensometer with 50 mm gauge length was adopted to measure the longitudinal strain of the coupons. During the tests, the applied load and strains were recorded at regular intervals by a data acquisition system. Additionally, the loading was paused for 100 seconds near the 0.2% proof stress and ultimate tensile strength, in accordance with the recommendations by Huang and Young [61] to allow for the stress relaxation. The meticulous approach herein has been employed in a sequence of tension coupon tests detailed in prior research [62-69].

Fig. 6 displays the stress-strain curves of WAAM 316L austenitic stainless steel specimens with different test orientations derived from the coupon tests, while Table 3 summarizes the corresponding material properties parameters. It is evident that tensile coupon specimens with orientations of $\theta = 0°$ and 90° exhibited comparatively weaker mechanical properties in terms of the elastic modulus and material strengths, when compared to specimens with other orientations. It is noteworthy that the stress-strain curves of the unmachined coupon specimens are lower than those of their machined counterparts. This trend is particularly pronounced for coupon specimens with $\theta = 90°$, aligning with findings in relevant literature [29, 53]. The anisotropy of unmachined WAAM austenitic stainless steel is more pronounced due to the geometric undulations featured by crest and trough regions, which are likely to experience stress concentration and localized deformation at the weakest cross-section [48, 49]. The inherent material anisotropy of WAAM austenitic stainless steel is a factor that merits consideration in future numerical investigations [70-72].

3. Single-lap shear tests

3.1. Test Setup

All single-lap shear bolted connections were tested using an electro-hydraulic servo-controlled testing machine. Details of test setup are shown in Fig. 7. The single shear bolted connections composed of a WAAM austenitic stainless steel sheet and an 8 mm thick Q960 high strength steel partner plate, affixed using a single fully threaded bolt. The partner plate had a higher nominal yield strength of 960MPa and larger thickness, ensuring failure to occur in the weaker WAAM austenitic stainless steel plate. Grade 12.9 high strength steel bolt with the size of M18 was used for single shear bolted connections, except that M24 bolt was used for UM-0-2.0-2.0, UM-0-2.0-1.5, UM-90-2.0-2.0 and UM-90-2.0-1.5 specimens, in order to mitigate the shear failure of bolt. All connections had a nominal bolt hole clearance of 2mm as per prEN 1993-1-8 [50]. Each bolt was hand-tightened to make light contact with the specimen surfaces, facilitating load transfer primarily through bearing while disregarding frictional effects. No washer was utilized to allow for curl-bearing failure, which is prone to occur in single shear connections consisting of thin-walled ductile plate [34, 42]. To mitigate the eccentricity effect during loading, a Q960 shim plate at the WAAM specimen end and a WAAM shim plate at the Q960 partner plate end with the same thickness were used at the clamping regions. Longitudinal displacement of bolted connection was captured by a LVDT. Monotonic tensile loading was applied utilizing a displacement-controlled pattern, with a constant rate of 1.0 mm/min.

3.2. Results and discussions

3.2.1. General

The observed failure patterns of all WAAM austenitic stainless steel single shear bolted connection tested specimens are reported in Table 4, where NSF denotes net section fracture, SF denotes shear-out failure, LTF denotes localized tearing failure, CBF denotes curl-bearing failure, additional letter ‘C’ in bracket denotes end curling. The typical failure patterns and the corresponding

load-deformation curves are demonstrated in Fig. 8 to Fig. 11. The prEN 1993-1-4 [51] defines the resistance of bolted connections separately by the deformation and strength criteria. Snijder *et al.* [73] also underscored the need to set a deformation limit for bolted connections. The consideration of deformation criterion is especially necessary for bolted connections with high ductility materials, such as WAAM austenitic stainless steel specimens investigated herein. In this study, the resistances of bolted connections determined by deformation criterion (P^d) for specimens not subjected to net section failure were obtained based on a deformation limit of 3.0 mm as recommended by Salih *et al.* [39] for austenitic stainless steel bolted connections. The resistances of bolted connections determined by strength criterion (P^s) defined as the ultimate strength were also obtained. The resistance of each specimen determined by two criteria are reported in Table 4. Detailed discussions on the failure modes and the influence of material anisotropy are included in the following sections.

3.2.2. Net section fracture (NSF) and localized tearing failure (LTF)

Net section fracture occurred in the bolted connections with relatively large end distance and narrow width that prone to necking. For the connection specimens failed by NSF, the post-yielding behavior is dependent on both the net cross-section area and material characteristics. In contrast to carbon steel that generally has a low tensile strength to yield strength ratio, the WAAM austenitic stainless steel featured a high tensile strength to yield strength ($\sigma_u/\sigma_{0.2}$) ratio exceeding 1.5 as shown in Table 3, leading to a notably ductile load-deformation response (Fig. 8 (a)) and effective stress redistribution across the net section for austenitic stainless steel bolted connections. It should be noted that the unmachined specimens UM-0-2.0-0.8 and UM-90-2.0-0.8 with larger effective plate thickness failed in NSF pattern, whilst the machined counterparts with smaller plate thickness experienced failure in the NSF(C) pattern, characterized by a combination of NSF and a significant degree of out-of-plane end curling (Fig. 8 (b)).

The localized tearing failure (LTF) usually occurred in the single shear bolted connections with substantial end distance and adequate width to prevent necking. This failure pattern was identified by

Rogers and Hancock [74] and has been frequently confused with NSF. The load-deformation curves for specimens subjected to LTF (Fig. 9 (a)) demonstrate considerably more ductile behavior than those subjected to NSF. As shown in Fig. 8 (b), one or two tearing cracks were initiated from the center of the hole and propagated nearly perpendicular to the loading direction, rather than necking cracks on the net section for NSF (see Fig. 9 (b)). All WAAM austenitic stainless steel single shear bolted connections in this study, irrespective of whether machined or unmachined, demonstrated significant out-of-plane end curling when failed in LTF pattern.

3.2.3. Shear-out failure (SF) and curl-bearing failure (CBF)

As summarized in Table 4, the shear-out failure (SF) pattern usually occurred in single shear WAAM austenitic stainless steel bolted connections with sufficient width and a relatively small end distance (mainly when $e_1'/d_0 \leq 2.0$). The WAAM sheet resisted the compressive stress by forming a tensile arc on the downstream side of the bolt. This was accompanied by noticeable material piling in front of the bolt and a protrusion at the end of the sheet in the direction of the applied force as illustrated in Fig. 10 (c). Connections failing in SF pattern exhibited significantly more ductile response compared to connections failing in NSF pattern, as evidenced by the corresponding load-displacement curves shown in Fig. 8 and Fig. 10. It was found that unmachined WAAM specimens with larger effective thickness and machined specimens with smaller thickness and small end distance (e.g. $e_1' = 1.0d_0$) failed in pure SF pattern. The out-of-plane curling phenomenon intensified as the end distance increased. As a result, it was observed from the test results that machined specimens with larger end distance failed in SF(C) pattern, characterized by a combination of SF and out-of-plane end curling as shown in Fig. 10 (c).

For thin-walled single shear bolted connections with ample width and larger end distance ($e_1' > 2.0d_0$), bearing failure accompanied by end curling (curl-bearing failure, CBF) occurred instead of pure bearing failure. The load-deformation response of bolted connections failed in CBF pattern remained rather ductile as demonstrated in Fig. 11 (a-c). The load increased swiftly with deformation

until the curling initiated at the free end of the WAAM sheet, which typically resulted in a minor load reduction. In the subsequent phase, the load experienced a gradual increase as the out-of-plane curling deformation intensified in conjunction with the in-plane deformation, until the specimen reached the ultimate bearing strength. After that, the load decreased rapidly as displacement increased when the connection experienced substantial in-plane and out-of-plane deformations as shown in Fig. 11 (d). It is noteworthy that the stage of rapid load increase for WAAM austenitic stainless steel single shear bolted connections with test orientation of θ=0° was prolonged, compared to those loaded with other orientations. This prolongation was primarily due to the delay of end curling, which could potentially lead to a superior ultimate strength.

3.2.4. Influence of test orientation

The resistances of WAAM austenitic stainless steel bolted specimens were normalized by the plate thickness to facilitate a direct comparison. The normalized resistances of specimen at test orientation θ symbolized as N_θ^d and N_θ^s were determined in deformation and strength criteria, respectively, which were further divided by the normalized resistance of specimen with θ= 90° in the same specimen group (i.e. N_{90}^d and N_{90}^s, respectively). Table 5 shows the comparison results regarding N_θ^d/N_{90}^d and N_θ^s/N_{90}^s values. Table 6 summarizes the failure pattern of each WAAM austenitic stainless steel single shear bolted connection at different test orientations for direct comparison. It can be observed that the average values of N_θ^d/N_{90}^d ratio are 1.04, 0.98, 0.99 and 1.03, whilst the average values of N_θ^s/N_{90}^s ratio are 1.16, 0.99, 1.03 and 0.94 for specimens with θ= 0°, 30°, 45° and 60°, respectively. It indicates insignificant anisotropy in the WAAM austenitic stainless steel single shear bolted connection resistance in deformation criterion (maximum deviation less than 4% when θ = 0°) and slightly more anisotropy in connection resistance in strength criterion (maximum deviation up to 16% when θ= 0°). The results indicate that specimen with θ= 0° generally possessed higher resistances in both deformation and strength criteria than the counterparts with other test orientations. This agrees with the finding regarding the prolonged stage of rapid load increase

observed in the load-displacement curves of specimens with $\theta = 0°$ as shown in previous section.

Interestingly, it can be observed from Table 6 that the test orientation can sometimes alter the failure pattern of the unmachined specimen in the same group, while the failure pattern of machined specimens remains consistent. For instance, the failure modes of specimens in the M-2.0-2.0 and M-2.0-1.5 groups remained consistent, irrespective of the loading orientations. In contrast, specimens with $\theta = 90°$ in the groups of UM-2.0-2.0 and UM-2.0-1.5 predominantly displayed LTF failure pattern, while the counterparts with $\theta = 0°$ altered into CBF pattern. This can be primarily attributed to the fact that unmachined WAAM austenitic stainless steel sheet with $\theta = 90°$ had significantly lower material strengths compared to the counterpart with $\theta = 0°$ as indicated in Table 3 such that the tearing cracks were more prone to form for specimen with $\theta = 90°$, leading to failure in LTF pattern.

4. Evaluation on current design rules

4.1. General

Since there is no specific design guideline for WAAM austenitic stainless steel single shear bolted connections, codified design methods [50-52] and proposed design equations in existing literature [34, 42] that originally developed and calibrated for carbon steel and stainless steel bolted connections produced by traditional cold-forming or hot-rolling technology are employed to evaluate their applicability in predicting the WAAM austenitic stainless steel single shear bolted connections. The experimental resistances of WAAM 316L austenitic stainless steel single shear bolted connections obtained in this study were compared with the resistances predicted by abovementioned design methods. The measured geometric dimensions and the measured tensile strength for the corresponding loading direction and surface finish were used in the design lap shear strength calculations of the connections, as per [42-44]. The safety factors were set equal to unity for the presented comparisons.

4.2. ANSI/AISC 370-21 [52]

The American Specification ANSI/AISC 370-21 [52] provides design provisions on the bearing and shear-out resistances of stainless steel connections considering both deformation and strength criteria. The design equations take hole deformation into account, but do not differentiate between single-lap and double-lap shear bolted connections. The bearing and shear-out resistances under the deformation criterion based on ANSI/AISC 370-21 [52] ($P^d_{b,AISC}$ and $P^d_{s,AISC}$) can be calculated as per Eqs. (1) and (2), respectively, whilst those under the strength criterion ($P^s_{b,AISC}$ and $P^s_{s,AISC}$) are calculated as per Eqs. (3) and (4), where *d* is the diameter of the bolt. The net section tensile resistance calculation specified in ANSI/AISC 370-21 [52] ($P_{n,AISC}$) is shown in Eq. (5), where the shear lag factor (U) is set as 1.0 for flat sheet connection and A_{net} is the corresponding net section area. The net section tensile resistance shall be calculated when determining the resistance of bolted connections under strength criterion, but not deformation criterion. The resistances of bolted connections predicted by ANSI/AISC 370-21 [52] under deformation and strength criteria (P^d_{AISC} and P^s_{AISC}) are determined by the minimum value of bearing resistance, shear-out resistance and net section tensile resistance (only for strength criterion).

$$P^d_{b,AISC} = 1.25dt\sigma_u \tag{1}$$

$$P^d_{s,AISC} = 1.25\left(\frac{e_1}{2d_0}\right)dt\sigma_u \tag{2}$$

$$P^s_{b,AISC} = \begin{cases} 2.5dt\sigma_u & \text{for } \frac{e_2}{d_0} > 1.5 \\ 2.0dt\sigma_u & \text{for } \frac{e_2}{d_0} \leq 1.5 \end{cases} \tag{3}$$

$$P^s_{s,AISC} = 2.5\left(\frac{e_1}{3d_0}\right)dt\sigma_u \tag{4}$$

$$P_{n,AISC} = UA_{net}\sigma_u \tag{5}$$

4.3. prEN 1993-1-8 [50]

Net section checking is required for bolted connection resistance design as specified in the

Chapter 5.5.1 of prEN 1993-1-8 [50]. The net section tensile resistance calculation ($P_{n,EC3-8}$) is specified in the Chapter 8.2.3 of prEN 1993-1-1 [75] as shown in Eq. (6), where k=1.0 for connections subjected to static loads and with smooth holes (e.g., fabricated by drilling or water cutting). The bearing resistance of lap-shear bolted connections ($P_{b,EC3-8}$) is calculated according to the Chapter 5.7 of prEN 1993-1-8 [50] as shown in Eq. (7), where the effect of edge distance considered in existing EN 1993-1-8 [76] is disregarded. This may be to prevent unnecessary reduction of resistance when the edge distance is small, as previously reported by Može's group [77, 78]. In Eq. (7), k_m denotes the parameter associated with steel grade and is taken as 1.0 as the yield strength of WAAM austenitic stainless steel in this study is less than 460MPa, α_b is determined according to Eq. (8), where σ_{ub} is the ultimate strength of bolt. It should be noted that prEN 1993-1-8 [50] does not impose a limit for bolt hole deformation regarding the connection resistance calculation. The resistance calculation does not differentiate between single-lap and double-lap shear bolted connections. The resistance of bolted connection predicted by prEN 1993-1-8 [50] (P^s_{EC3-8}) is determined by the minimum value of net section tensile resistance and bearing resistance as calculated by Eq. (6) and Eq. (7), respectively.

$$P_{n,EC3-8} = k\sigma_u A_{net} \tag{6}$$

$$P_{b,EC3-8} = k_m \alpha_b \sigma_u d \tag{7}$$

$$\alpha_b = min\left\{\frac{e_1}{d_0},\ 3\frac{\sigma_{ub}}{\sigma_u},\ 3.0\right\} \tag{8}$$

4.4. prEN 1993-1-4 [51]

The resistances of stainless steel bolted connections specified in the Chapter 10.2 of prEN 1993-1-4 [51] are determined by both strength criterion and deformation criterion (considering the deformation of the bolt hole), denoted as P^s_{EC3-4} and P^d_{EC3-4}, respectively. The resistance calculation equation specified in prEN 1993-1-4 [51] is independent of the failure pattern and the unified equation is shown in Eq. (9), where α_b and k_1 are the bearing coefficients parallel and perpendicular to the loading direction, respectively. To determine the connection resistance in strength

criterion (P^{s}_{EC3-4}), the values of bearing coefficients parallel and perpendicular to the loading direction are determined by Eqs. (10) and (11). Whilst to determine the connection resistance in deformation criterion (P^{d}_{EC3-4}), the value of bearing coefficient parallel to the loading direction determined by Eq. (12) together with the value of k_1^d equal to 0.5 is adopted.

$$P_{EC3-4} = k_1 \alpha_b \sigma_u dt \tag{9}$$

$$\alpha_b^s = \begin{cases} \min\left\{\frac{5e_1}{4d_0},\ 2.5\right\} & \text{for } t \le 4 \\ \min\left\{\frac{5e_1}{6d_0},\ 2.5\right\} & \text{for } t > 4 \end{cases} \tag{10}$$

$$k_1^s = \begin{cases} 0.64 & \text{for } t \le 4 \\ 1.0 & \text{for } \frac{e_2}{d_0} > 1.5 \text{ and } t > 4 \\ 0.8 & \text{for } \frac{e_2}{d_0} \le 1.5 \text{ and } t > 4 \end{cases} \tag{11}$$

$$\alpha_b^d = \min\left\{\frac{5e_1}{4d_0},\ 2.5\right\} \tag{12}$$

It is worth mentioning that, the design approach provided by prEN 1993-1-4 [51] is identical to that in the design manual for structural stainless steel SCI P413 [79]. Moreover, the calculation of P^{d}_{EC3-4} is exactly the same as the connection resistance calculation as per AISC 370-21 [52] in deformation criterion (P^{d}_{AISC}). Therefore, the values of P^{d}_{EC3-4} are not shown in Table 4 for simplicity.

4.5. Design equations by Teh's Group [34, 42]

Different from double shear bolted connection, single shear bolted connection with small plate thickness and certain range of end distance might be prone to end curling, which affects the resistance of bolted connection. By considering possible end curling effect for single shear bolted connection, Teh and Uz [34] have proposed a tilt-bearing resistance equation as shown in Eq. (13).

$$P_{t,Teh} = 2.65 d^{1/2} t^{4/3} (b - d_0)^{1/6} \sigma_u \tag{13}$$

This equation was initially developed for the tilt-bearing resistance calculation of cold-reduced steel single-lap bolted connections, and has been further employed and validated by Guo *et al.* [42] for WAAM carbon steel single-lap bolted thin sheet failed in localized tearing and curl-bearing

patterns (LTF and CBF). For connections failed by shear-out pattern, the resistance of bolted connection is calculated by Eq. (14) as per Guo *et al.* [42], where l_{av} denotes the length of active shear plane (=e_1-d_0/4). Only the strength criterion is considered. The resistance of bolt connection (P_{Teh}^{S}) equals to $P_{t,Teh}$ for connections failed by LTF and CBF patterns, and $P_{s,Guo}$ for connections failed by SF pattern.

$$P_{s,Guo} = 1.2\left(\frac{3d}{e_1}\right)^{0.1} l_{av} t \sigma_u \tag{14}$$

5. Design strength comparisons

Experimental resistances determined by deformation criterion (P^d) were compared with predictions using the American Standard ANSI/AISC 370-21 [52] (P_{AISC}^{d}), while the resistances determined by strength criterion (P^s) were compared with predictions using the ANSI/AISC 370-21 [52] (P_{AISC}^{S}), the Eurocode 3 prEN 1993-1-8 [50] (P_{EC3-8}^{S}) and prEN 1993-1-4 [51] (P_{EC3-4}^{S}), as well as design equations proposed by Teh's Group [34, 42] (P_{Teh}^{S}), as delineated in Table 4.

Among the design rules considered in this study, only the American Standard ANSI/AISC 370-21 [52] and Eurocode 3 prEN 1993-1-4 [51] take into account the effect of the bolt hole deformation limit and consider the deformation criterion in the resistance calculation of connections. The mean value of test-to-predicted strength ratio is 1.29 with a COV of 0.109. This indicates that both standards offer conservative resistance predictions for WAAM 316L austenitic stainless steel single shear bolted connections in deformation criterion.

In terms of the resistance in strength criterion, both ANSI/AISC 370-21 [52] and prEN 1993-1-4 [51] yield overly conservative predictions, evident by the mean value of P^s/P_{AISC}^{S} = 1.24 with CoV = 0.217 and the mean value of P^s/P_{EC3-4}^{S} = 1.51 with CoV = 0.167, respectively. Regarding design predictions by prEN 1993-1-8 [50], the mean value of P^s/P_{EC3-8}^{S} = 1.06 with CoV = 0.207. It was found that the end-curling effect would affect the connection resistance for single shear bolted connection. However, the resistance calculations in these design provisions do not properly consider

the effect of failure pattern on the resistance for single shear bolted connection, which might lead to the scattered design predictions [54, 80]. Design equations proposed by Teh's Group [34, 42] consider the possible end curling effect of single shear bolted connection. The strength predictions are less scattered as evident by the mean value of P^s/P^s_{Teh} = 1.16 and CoV = 0.119. Further study is needed to improve the accuracy of strength predictions for WAAM 316L austenitic stainless steel single shear bolted connections.

6. Conclusions

This study provides profound insights into the behavior of WAAM 316L austenitic stainless steel single shear bolted connections. Through tensile tests on 44 WAAM austenitic stainless steel single shear bolted connections, the influences of bolt hole position, WAAM sheet surface geometric undulation, and loading orientation on the structural behavior of connections were examined. In light of the absence of codified design provisions for WAAM stainless steel bolted connections, the feasibility of existing design rules originally developed for bolted connections produced by traditional carbon steel and stainless steel was checked. The following conclusions can be obtained.

i) Net section fracture with/without end curling (NSF(C) and NSF), local tearing failure (LTF), shear-out failure with/without end curling (SF(C) and SF), and curl-bearing failure (CBF) were identified as typical failure patterns in WAAM 316L austenitic stainless steel single shear bolted connections. All failure patterns are classified as bearing type, except for the NSF(C) and NSF patterns.

ii) For WAAM austenitic stainless steel single shear bolted connections with substantial end distance and narrow width, net section fracture characterized by the necking of net cross-section, and local tearing failure characterized by two tearing cracks initiating from the center of the hole together with end curling, were observed. For connections with ample width and relatively small end distance, shear-out failure pattern was found, whilst curl-bearing failure pattern was found in connections with ample width and large end distance. Connections failed in bearing type patterns

exhibited more ductile responses than those failed in NSF pattern.

iii) The test orientation had little effect on the structural performance of WAAM 316L austenitic stainless steel single shear bolted connections regarding the connection resistance and deformation response. Nonetheless, the test orientation could sometimes influence the failure pattern of bolted connections.

iv) Among the current design rules for bolted connections evaluated in this study, the design guidelines of ANSI/AISC 370-21 [52] and prEN 1993-1-4 [51] offer conservative resistance predictions in deformation criterion. Design equations by Teh's Group [34, 42] provide the least scattered resistance predictions in strength criterion, whilst the Eurocode prEN 1993-1-8 [50] provides the most accurate resistance predictions despite a certain degree of scatter. However, further study shall be conducted to improve the accuracy of strength predictions for WAAM austenitic stainless steel bolted connections.

Acknowledgements

The authors are grateful to Rongsu Technology Ltd. in China for supplying the test specimens. The authors are also thankful to Dr. Jingjing Zhang from the Engineering Mechanics Experimental Center of Shanghai Jiao Tong University for her assistance in the experimental program. The authors would also like to thank the support from the National Natural Science Foundation of China (No. 52378167 and No. 52108157) and the SJTU Global Strategic Partnership Fund (2023 SJTU-UoE).

Data Availability Statement

All data, models, and code generated or used during the study are available upon reasonable request.

References

[1] Chen M-T, Zuo W, Young B. Tests of cold-formed steel T-joints with semi-oval hollow section chord. Journal of Structural Engineering 2023;149(8):04023099.

[2] Chen M-T, Chen Y, Young B. Static strengths of cold-formed steel elliptical hollow section X-joints. Thin-Walled Structures 2023;191:110997.

[3] Su AD, Zhao O. Experimental and numerical investigations of S960 ultra-high strength steel slender welded I-section columns failing by local-flexural interactive buckling. Thin-Walled Structures 2022;180:109898.

[4] Lai MH, Song W, Ou XL, Chen MT, Wang Q, Ho JCM. A path dependent stress-strain model for concrete-filled-steel-tube column. Engineering Structures 2020;211:110312.

[5] Ke K, Zhang H, Zhou X, Yam MCH, Wang Y, Shi T. Hybrid-self-centring steel frames: Insights and probabilistic seismic assessment. Engineering Structures 2024;303:117516.

[6] Zuo W, Chang H, Li Z, An A, Xia J, Yu T. Experimental investigation on compressive behavior of corroded thin-walled CHS T-joints with grout-filled GFRP tube repairing. Thin-Walled Structures 2022;175:109222.

[7] Chang H, Zuo W, Yang J, Song X, Huang Y. Compressive strength of collar plate reinforced SHS T-joints: Effect of geometrical parameters and chord stress ratio. Journal of Constructional Steel Research 2020;174:106278.

[8] Chang H, Zuo W, Xia J, Xu B, Ma R, Zhang L. Sensitivity analysis of geometrical design parameters on the compressive strength of the vertical inner-plate reinforced square hollow section T-joints: A finite element study. Engineering Structures 2020;208:110308.

[9] Su AD, Jiang K, Wang MD, Zhao O. S960 ultra-high strength steel slender welded I-section beam-columns: Testing, numerical modelling and design. Thin-Walled Structures 2022;177:109452.

[10] Wang HT, Bian ZN, Chen MS, Hu LL, Wu Q. Flexural strengthening of damaged steel beams with prestressed CFRP plates using a novel prestressing system. Engineering Structures 2023;284.

[11] Chang H, Yan X, Zuo W, Xia J, Yu T. Numerical analysis and design methods of grout-filled GFRP tube repaired corroded CHS T-joints. Thin-Walled Structures 2024;198:111719.

[12] Zhou X, Huang Y, Ke K, Yam MCH, Zhang H, Fang H. Large-size shape memory alloy plates subjected to cyclic tension: Towards novel self-centring connections in steel frames. Thin-Walled Structures 2023;185:110591.

[13] Chen M-T, Young B. Tensile tests of cold-formed stainless steel tubes. Journal of Structural Engineering 2020;146(9):04020165.

[14] Wang YJ, Su AD, Yang H, Zhao J, Wang YY. S890 hot-rolled ultra-high strength steel (UHSS) seamless circular hollow section beam-columns: Testing, modelling and design. Thin-Walled Structures 2024;197:111583.

[15] Su AD, Wang YY, Wang YJ, Rasmussen KJR, Gardner L. Behaviour and design of S960 ultra-high strength steel non-slender welded I-section beam-columns. Engineering Structures 2024;304:117602.

[16] Su A, Yang H, Wang Y, Wang Y. Experimental and numerical investigations of S960 hot-rolled ultra-high strength steel seamless circular hollow section beam–columns. Thin-Walled Structures 2024;200:111909.

[17] Cheng B, Huang F, Duan Y, Chen M-T. Fatigue performance of bird-beak SHS gap K-joints under brace in-plane force. Journal of Structural Engineering 2021;147(11):04021167.

[18] Chen M-T, Young B. Beam-column design of cold-formed steel semi-oval hollow non-slender sections. Thin-Walled Structures 2021;162:107376.

[19] Chen M-T, Young B. Numerical analysis and design of cold-formed steel elliptical hollow sections under combined compression and bending. Engineering Structures 2021;241:112417.

[20] Chen M-T, Young B. Tests of cold-formed steel semi-oval hollow section members under eccentric axial load. Journal of Structural Engineering 2020;146(4):04020027.

[21] Chen M-T, Young B. Beam-column tests of cold-formed steel elliptical hollow sections. Engineering Structures 2020;210:109911.

[22] Zuo W, Chen M-T, Young B. Post-fire behaviour of cold-formed steel semi-oval hollow section stub columns. Journal of Structural Engineering 2024:https://doi.org/10.1061/JSENDH/STENG-13392.

[23] Zuo W, Chen M-T, Young B. Structural behaviour of cold-formed steel elliptical hollow section stub columns after exposure to ISO-834 fire curve. Thin-Walled Structures 2024;197:111309.

[24] Wang J, Ke K, Yam MCH, Teng M, Wang W. Improving structural robustness of steel frame buildings by enhancing floor deck connections. Journal of Constructional Steel Research 2023;204:107842.

[25] Tian SY, Wu JL, Mo JX, Lai CL, Ren FM, Lai MH. Seismic behaviour of a novel demountable joint connecting FTCES columns and RC beams. Structures 2023;54:746-763.

[26] Ren FM, Tian SY, Gong L, Wu JL, Mo JX, Lai CL, Lai MH. Seismic performance of a ring beam joint connecting FTCES column and RC/ESRC beam with NSC. Journal of Building Engineering 2023;63:105366.

[27] Chen M-T, Zuo W, Chen Y, Zhao O, Cheng B, Zhao J. Parametric topology optimization design and analysis of additively manufactured joints in spatial grid structures. Engineering Structures 2024;300:117123.

[28] Zuo W, Chen M-T, Chen Y, Zhao O, Cheng B, Zhao J. Additive manufacturing oriented parametric topology optimization design and numerical analysis of steel joints in gridshell structures. Thin-Walled Structures 2023;188:110817.

[29] Hadjipantelis N, Weber B, Buchanan C, Gardner L. Description of anisotropic material response of wire and arc additively manufactured thin-walled stainless steel elements. Thin-Walled Structures 2022;171:108634.

[30] Wang Z, Hou Y, Huang C, Han Q, Zong L, Chen M-T, Deng K, Gardner L. Experimental study and constitutive modelling of wire arc additively manufactured steel under cyclic loading. Journal of Constructional Steel Research 2024;213:108420.

[31] Buchanan C, Gardner L. Metal 3D printing in construction: A review of methods, research, applications, opportunities and challenges. Engineering Structures 2019;180:332-348.

[32] Guo X, Kyvelou P, Ye J, Gardner L. Experimental investigation of wire arc additively manufactured steel T-stub connections. Journal of Constructional Steel Research 2023;211:108106.

[33] Teh LH, Gilbert BP. Net Section Tension Capacity of Bolted Connections in Cold-Reduced Steel Sheets. Journal of Structural Engineering 2012;138(3):337-344.

[34] Teh LH, Uz ME. Ultimate Tilt-Bearing Capacity of Bolted Connections in Cold-Reduced Steel Sheets.

Journal of Structural Engineering 2017;143(4):04016206.

[35] Guo HC, Xiao F, Liu YH, Liang G. Experimental and numerical study on the mechanical behavior of Q460D high-strength steel bolted connections. Journal of Constructional Steel Research 2018;151:108-121.

[36] Wang YB, Lyu YF, Li GQ, Liew JYR. Behavior of single bolt bearing on high strength steel plate. Journal of Constructional Steel Research 2017;137:19-30.

[37] Jiang K, Zhao O, Tan KH. Experimental and numerical study of S700 high strength steel double shear bolted connections in tension. Engineering Structures 2020;225:111175.

[38] Jiang K, Zhao O. Ferritic stainless steel thin sheet bolted connections failing by bearing-curling interaction: Testing, modelling and design. Engineering Structures 2023;283:115919.

[39] Salih EL, Gardner L, Nethercot DA. Bearing failure in stainless steel bolted connections. Engineering Structures 2011;33(2):549-562.

[40] Kim TS, Kuwamura H, Kim S, Lee Y, Cho T. Investigation on ultimate strength of thin-walled steel single shear bolted connections with two bolts using finite element analysis. Thin-Walled Structures 2009;47(11):1191-1202.

[41] Sobrinho KD, da Silva AT, Rodrigues MC, Henriques JA, Vellasco PCGD, de Lima LRO. A comprehensive assessment of curling effects in stainless steel bolted connections. Thin-Walled Structures 2022;176:109387.

[42] Guo X, Kyvelou P, Ye J, Teh LH, Gardner L. Experimental investigation of wire arc additively manufactured steel single-lap shear bolted connections. Thin-Walled Structures 2022;181:110029.

[43] Guo X, Kyvelou P, Ye J, Teh LH, Gardner L. Experimental study of DED-arc additively manufactured steel double-lap shear bolted connections. Engineering Structures 2023;281:115736.

[44] Ye J, Liu Y, Yang Y, Wang Z, Zhao O, Zhao Y. Testing, analysis and design of wire and arc additively manufactured steel bolted connections. Engineering Structures 2023;(296):116939.

[45] Liu Y, Ye J, Yang Y, Quan G, Wang Z, Zhao W, Zhao Y. Experimental study on wire and arc additively manufactured steel double-shear bolted connections. Journal of Building Engineering 2023;76:107330.

[46] Huang C, Kyvelou P, Gardner L. Stress-strain curves for wire arc additively manufactured steels. Engineering Structures 2023;279:115628.

[47] Gardner L. Metal additive manufacturing in structural engineering-review, advances, opportunities and outlook. Structures 2023;47:2178-2193.

[48] Chen M-T, Zhang T, Gong Z, Zuo W, Wang Z, Zong L, Zhao O, Hu L. Mechanical properties and microstructure characteristics of wire arc additively manufactured high-strength steels. Engineering Structures 2024;300:117092.

[49] Chen M-T, Gong Z, Zhang T, Zuo W, Zhao Y, Zhao O, Zhang G, Wang Z. Mechanical behavior of austenitic stainless steels produced by wire arc additive manufacturing. Thin-Walled Structures 2024;196:111455.

[50] prEN 1993-1-8:2021. Eurocode 3: Design of steel structures — Part 1-8: Design of joints. Brussels, Belgium: CEN (European Committee for Standardization); 2021.

[51] prEN 1993-1-4:2023. Eurocode 3: Design of steel structures — Part 1-4: Stainless steels. Brussels, Belgium: CEN (European Committee for Standardization); 2023.

[52] ANSI/AISC 370-21. Specification for Structural Stainless Steel Buildings. Chicago: AISC (American Institute of Steel Construction); 2021.

[53] Kyvelou P, Slack H, Mountanou DD, Wadee MA, Ben Britton T, Buchanan C, Gardner L. Mechanical and microstructural testing of wire and arc additively manufactured sheet material. Materials & Design 2020;192:108675.

[54] Kim TS, Yoo J, Roeder CW. Experimental investigation on strength and curling influence of bolted connections in thin-walled carbon steel. Thin-Walled Structures 2015;91:1-12.

[55] Kim TS, Kuwamura H, Cho TJ. A parametric study on ultimate strength of single shear bolted connections with curling. Thin-Walled Structures 2008;46(1):38-53.

[56] Geomagic Design X. Geomagic Design X (version 2022.0.0). Oqton, Inc.; 2022.

[57] Rhinoceros-3D. Rhinoceros 3D (Version 8.0). Robert McNeel & Associates, (TLM, Inc.). USA; 2024.

[58] Grasshopper. Grasshopper (Version 1.0). Robert McNeel & Associates, (TLM, Inc.). USA; 2024.

[59] Chen M-T, Chen Y, Zuo W, Yun X, Zhao O, Liu S-W, Xu F. Experimental investigation on the tensile behavior of wire arc additively manufactured duplex stainless steel plates. 2024;(In preparation).

[60] ASTM E8/E8M − 22. Standard Test Methods for Tension Testing of Metallic Materials. West Conshohocken, USA: ASTM(American Society for Testing and Materials); 2022.

[61] Huang Y, Young B. The art of coupon tests. Journal of Constructional Steel Research 2014;96:159-175.

[62] Chen M-T, Pandey M, Young B. Mechanical properties of cold-formed steel semi-oval hollow sections after exposure to ISO-834 fire. Thin-Walled Structures 2021;167:108202.

[63] Chen M-T, Pandey M, Young B. Post-fire residual material properties of cold-formed steel elliptical hollow sections. Journal of Constructional Steel Research 2021;183:106723.

[64] Zhang T, Chen M-T, Cai A, Cao H, Yun X, Zhao H, Shen C, Zhang Y. Behaviour of high strength steel butt joints exposed to arctic low temperatures. Thin-Walled Structures 2023;192:111157.

[65] Yi S, Chen M-T, Young B. Design of concrete-filled cold-formed steel elliptical stub columns. Engineering Structures 2023;276:115269.

[66] Yi S, Chen M-T, Young B. Stub column behavior of concrete-filled cold-formed steel semi-oval sections. Journal of Structural Engineering 2023;149(3):04023001.

[67] Chen M-T, Cai A, Pandey M, Shen C, Zhang Y, Hu L. Mechanical properties of high strength steels and weld metals at arctic low temperatures. Thin-Walled Structures 2023;185:110543.

[68] Chen M-T, Zhang T, Young B. Behavior of concrete-filled cold-formed steel built-up section stub columns. Thin-Walled Structures 2023;187:110692.

[69] Chen M-T, Young B, Martins AD, Camotim D, Dinis PB. Experimental investigation on cold-formed steel lipped channel beams affected by local-distortional interaction under non-uniform bending. Thin-Walled Structures 2021;161:107494.

[70] Song YC, Lin XM, Yam MCH, Ke K, Wang J. Behaviour and design of duplex stainless steel bolted connections failing in block shear. Engineering Structures 2024;302:117442.

[71] Lin XM, Yam MCH, Song YC, Chung KF, Ho HC, Han YW. Net section tension capacity of high strength steel single shear bolted connections. Thin-Walled Structures 2024;195:111371.

[72] Song YC, Lin XM, Yam MCH, Ke K. Block shear failure of austenitic stainless steel bolted connections. Thin-Walled Structures 2023;193:111251.

[73] Snijder H, Ungermann D, Stark J, Sedlacek G, Bijlaard F, Hemmert-Halswick A 1988. Evaluation of test results on bolted connections in order to obtain strength functions and suitable model factors-part A: results. *Eurocode No.3 - part 1 - background documentation. Document 6.01.* Brussels: Commission of the European Communities.

[74] Rogers CA, Hancock GJ. Failure modes of bolted-sheet-steel connections loaded in shear. Journal of Structural Engineering 2000;126(3):288-296.

[75] prEN 1993-1-1:2020. Eurocode 3: Design of steel structures — Part 1-1: General rules and rules for buildings. Brussels, Belgium: CEN (European Committee for Standardization); 2020.

[76]EN 1993-1-8:2005. Eurocode 3: Design of steel structures — Part 1-8: Design of joints. Brussels, Belgium: CEN (European Committee for Standardization); 2005.

[77] Može P, Beg D. A complete study of bearing stress in single bolt connections. Journal of Constructional Steel Research 2014;95:126-140.

[78] Može P. Bearing strength at bolt holes in connections with large end distance and bolt pitch. Journal of Constructional Steel Research 2018;147:132-144.

[79] SCI P413. Design Manual for Structural Stainless Steel – 4th Edition. Berkshire, UK: SCI (The Steel Construction Institute); 2018.

[80] Kim G, Kim T, Hwang B, Kim J. Ultimate strength of lean duplex stainless steel single-shear bolted connections with four bolts. Thin-Walled Structures 2020;155:106950.

Tables

Table 1 Chemical composition of ER316L austenitic stainless steel feedstock wire provided by the manufacturer (values in %)

C	Mn	Si	P	Ni	Cr	Cu	Mo	S
0.011	2.00	0.60	0.02	11.70	19.00	0.05	2.15	0.011

Table 2 Measured geometric properties of WAAM austenitic stainless steel sheets for bolted connection specimens

Label	b (mm)	t (mm)	d_0 (mm)	e_1 (mm)	e_2 (mm)	e_1/d_0	e_2/d_0
M-0-1.0-3.0	140.53	3.28	19.47	19.85	60.53	1.52	3.61
M-0-1.5-3.0	140.58	3.42	19.53	29.86	60.53	2.03	3.60
M-0-2.0-3.0	140.14	3.41	19.62	39.96	60.26	2.54	3.57
M-0-2.5-3.0	140.73	3.48	19.85	49.89	60.44	3.01	3.54
M-0-3.0-3.0	140.24	3.42	19.49	60.38	60.38	3.60	3.60
M-0-4.0-3.0	140.47	3.34	19.69	80.49	60.39	4.59	3.57
M-45-1.0-3.0	140.05	3.47	19.63	19.87	60.21	1.51	3.57
M-45-1.5-3.0	139.90	3.37	19.70	29.78	60.10	2.01	3.55
M-45-1.5-3.0R	140.17	3.40	19.65	29.70	60.26	2.01	3.57
M-45-2.0-3.0	139.75	3.40	19.59	39.95	60.08	2.54	3.57
M-45-2.5-3.0	140.05	3.41	19.62	50.04	60.22	3.05	3.57
M-45-3.0-3.0	140.12	3.50	19.69	60.31	60.72	3.73	3.75
M-45-4.0-3.0	140.30	3.47	19.57	79.82	60.37	4.58	3.58
M-90-1.0-3.0	139.93	3.35	19.66	19.89	60.14	1.51	3.56
M-90-1.5-3.0	140.52	3.41	19.71	29.70	60.41	2.01	3.56
M-90-1.5-3.0R	140.24	3.28	19.65	29.75	60.30	2.01	3.57
M-90-2.0-3.0	140.41	3.40	19.61	39.85	60.40	2.53	3.58
M-90-2.5-3.0	140.00	3.33	19.57	50.35	60.22	3.07	3.58
M-90-3.0-3.0	140.70	3.42	19.62	59.63	60.54	3.54	3.59
M-90-4.0-3.0	139.75	3.56	19.80	80.60	59.98	4.57	3.53
M-30-1.5-3.0	139.84	3.68	19.62	30.04	60.11	2.03	3.56
M-30-1.5-3.0R	140.02	3.45	19.64	29.69	60.19	2.01	3.56
M-60-1.5-3.0	139.82	3.40	19.62	29.40	60.10	2.00	3.56
M-30-3.0-3.0	139.19	3.55	19.57	59.85	59.81	3.56	3.56
M-60-3.0-3.0	140.27	3.62	19.65	59.75	60.31	3.54	3.57
M-0-2.0-0.8	52.23	3.58	19.53	39.93	16.35	2.54	1.34
M-0-2.0-1.5	79.82	3.49	19.98	39.87	29.92	2.50	2.00
M-0-2.0-2.0	100.01	3.35	19.73	39.93	40.14	2.52	2.53
M-45-2.0-0.8	50.58	3.42	19.58	39.95	15.50	2.54	1.29
M-45-2.0-1.5	80.31	3.36	19.95	39.65	30.18	2.49	2.01
M-45-2.0-2.0	100.03	3.25	19.72	39.83	40.16	2.52	2.54
M-90-2.0-0.8	52.39	3.46	19.98	39.83	16.21	2.49	1.31
M-90-2.0-1.5	80.48	3.77	19.53	39.70	30.48	2.53	2.06
M-90-2.0-2.0	100.73	3.27	19.96	39.94	40.39	2.50	2.52
M-30-2.0-1.5	80.16	3.49	19.55	39.97	30.31	2.54	2.05
M-60-2.0-1.5	80.16	3.64	19.97	39.91	30.10	2.50	2.01
UM-0-1.5-3.0	140.11	6.32	19.87	29.54	60.12	1.99	3.53
UM-0-2.0-2.0	130.29	6.37	26.14	51.91	52.08	2.49	2.49
UM-0-2.0-1.5	104.07	6.47	26.10	51.97	38.99	2.49	1.99
UM-0-2.0-0.8	51.74	6.51	20.09	39.93	15.83	2.49	1.29
UM-90-1.5-3.0	139.89	6.61	19.98	29.79	59.96	1.99	3.50
UM-90-2.0-2.0	129.21	6.54	26.15	39.84	51.89	2.48	2.47
UM-90-2.0-1.5	103.92	6.47	25.93	52.32	39.00	2.52	2.00
UM-90-2.0-0.8	51.91	6.63	19.93	40.16	15.99	2.52	1.30

Table 3 Material properties of WAAM 316L austenitic stainless steel specimens

Coupon	E (GPa)	$\sigma_{0.2}$ (MPa)	ε_u (%)	σ_u (MPa)	ε_f (%)	$\sigma_u/\sigma_{0.2}$
M0	131.0	300.3	37.0	513.2	46.6	1.71
M30	163.1	355.8	24.3	550.0	26.4	1.55
M45	164.9	351.9	27.8	547.1	28.2	1.55
M60	194.0	348.7	29.0	535.2	30.0	1.53
M90	133.2	316.2	38.2	515.5	50.4	1.63
UM0	152.2	295.7	36.0	502.4	47.1	1.70
UM90	88.8	260.4	31.1	463.4	39.3	1.78

Table 4 Summary of test results and design comparisons for WAAM austenitic stainless steel single shear bolted connections

Specimen	Failure pattern	Deformation criterion		Strength criterion				
		P^d(kN)	$\frac{P^d}{P^d_{AISC}}$	P^s(kN)	$\frac{P^s}{P^s_{AISC}}$	$\frac{P^s}{P^s_{EC3-8}}$	$\frac{P^s}{P^s_{EC3-4}}$	$\frac{P^s}{P^s_{Teh}}$
M-0-1.0-3.0	SF	41.7	1.45	61.9	1.61	1.34	1.68	1.17
M-0-1.5-3.0	SF	57.2	1.45	97.2	1.82	1.52	1.92	1.29
M-0-2.0-3.0	CBF	53.3	1.35	97.9	1.47	1.23	1.94	1.03
M-0-2.5-3.0	CBF	58.4	1.45	91.4	1.14	0.95	1.78	1.38
M-0-3.0-3.0	CBF	57.3	1.45	91.2	1.15	0.96	1.80	1.41
M-0-4.0-3.0	CBF	55.5	1.44	81.2	1.05	0.88	1.64	1.29
M-45-1.0-3.0	SF	42.5	1.32	67.4	1.57	1.30	1.63	1.12
M-45-1.5-3.0	SF(C)	48.7	1.17	66.5	1.20	1.00	1.25	0.84
M-45-1.5-3.0R	SF(C)	50.4	1.20	70.1	1.25	1.04	1.31	0.88
M-45-2.0-3.0	CBF	49.8	1.19	74.5	1.05	0.88	1.39	1.09
M-45-2.5-3.0	CBF	51.5	1.23	78.7	0.94	0.78	1.46	1.14
M-45-3.0-3.0	CBF	56.7	1.32	76.5	0.89	0.74	1.39	1.07
M-45-4.0-3.0	CBF	54.1	1.27	76.1	0.89	0.74	1.39	1.08
M-90-1.0-3.0	SF	48.2	1.64	69.0	1.76	1.47	1.84	1.26
M-90-1.5-3.0	SF(C)	52.9	1.34	77.3	1.46	1.22	1.53	1.03
M-90-1.5-3.0R	SF(C)	52.8	1.39	79.5	1.56	1.30	1.63	1.10
M-90-2.0-3.0	CBF	53.0	1.34	72.1	1.08	0.90	1.43	1.12
M-90-2.5-3.0	CBF	53.0	1.37	69.9	0.90	0.75	1.41	1.11
M-90-3.0-3.0	CBF	53.6	1.35	81.1	1.02	0.85	1.60	1.24
M-90-4.0-3.0	CBF	43.9	1.06	82.9	1.00	0.84	1.57	1.21
M-30-1.5-3.0	SF	51.6	1.13	92.6	1.50	1.25	1.59	1.06
M-30-1.5-3.0R	SF	55.7	1.30	90.8	1.59	1.32	1.66	1.12
M-60-1.5-3.0	SF(C)	52.5	1.28	75.1	1.38	1.15	1.43	0.97
M-30-3.0-3.0	CBF	56.6	1.29	82.4	0.94	0.78	1.47	1.13
M-60-3.0-3.0	CBF	61.4	1.41	82.4	0.95	0.79	1.48	1.13
M-0-2.0-0.8	NSF(C)	---	---	64.0	1.08	1.08	1.21	---
M-0-2.0-1.5	LTF	55.9	1.39	88.4	1.37	1.10	1.71	1.49
M-0-2.0-2.0	SF(C)	56.9	1.47	102.1	1.57	1.31	2.06	1.09
M-45-2.0-0.8	NSF(C)	---	---	54.7	0.96	0.96	1.02	0.96
M-45-2.0-1.5	LTF	46.6	1.13	80.7	1.18	0.98	1.52	1.34
M-45-2.0-2.0	SF(C)	55.0	1.37	104.9	1.56	1.30	2.05	1.09
M-90-2.0-0.8	NSF(C)	---	---	63.1	1.09	1.09	1.23	---
M-90-2.0-1.5	LTF	57.3	1.31	85.3	1.16	0.96	1.52	1.29
M-90-2.0-2.0	SF(C)	52.5	1.38	69.9	1.10	0.92	1.44	1.22
M-30-2.0-1.5	LTF	54.6	1.26	69.8	0.95	0.79	1.26	1.10
M-60-2.0-1.5	LTF	55.3	1.26	73.1	1.00	0.83	1.30	1.12
UM-0-1.5-3.0	SF	78.9	1.11	152.5	1.61	1.34	1.61	1.12
UM-0-2.0-2.0	CBF	97.6	1.02	219.6	1.38	1.15	1.38	1.34
UM-0-2.0-1.5	CBF	97.8	1.00	204.9	1.31	1.05	1.27	1.28
UM-0-2.0-0.8	NSF	---	---	115.0	1.11	1.11	1.18	---
UM-90-1.5-3.0	SF	85.1	1.24	162.5	1.78	1.48	1.78	1.23
UM-90-2.0-2.0	LTF	102.0	1.08	179.7	1.19	0.99	1.19	1.15

UM-90-2.0-1.5	LTF	98.4	1.13	165.4	1.10	0.91	1.10	1.12
UM-90-2.0-0.8	NSF	---	---	109.3	1.11	1.11	1.18	---
Mean			1.29		1.24	1.06	1.51	1.16
Cov			0.109		0.217	0.207	0.167	0.119

Table 5 Effect of test orientation on resistances of WAAM austenitic stainless steel single shear bolted connections

Specimen group	0°		30°		45°		60°	
	N_0^d/N_{90}^d	N_0^s/N_{90}^s	N_{30}^d/N_{90}^d	N_{30}^s/N_{90}^s	N_{45}^d/N_{90}^d	N_{45}^s/N_{90}^s	N_{60}^d/N_{90}^d	N_{60}^s/N_{90}^s
M-1.0-3.0	0.88	0.92	---	---	0.85	0.94	---	---
M-1.5-3.0	1.08	1.25	0.90	1.11	0.93	0.87	1.00	0.97
M-2.0-3.0	1.00	1.35	---	---	0.94	1.03	---	---
M-2.5-3.0	1.05	1.25	---	---	0.95	1.10	---	---
M-3.0-3.0	1.07	1.12	1.02	0.98	1.03	0.92	1.08	0.96
M-4.0-3.0	1.35	1.04	---	---	1.26	0.94	---	---
M-2.0-0.8	---	0.98	---	---	---	0.88	---	---
M-2.0-1.5	1.05	1.12	1.03	0.88	0.91	1.06	1.00	0.89
M-2.0-2.0	1.06	1.43	---	---	1.05	1.51	---	---
UM-1.5-3.0	0.97	0.98	---	---	---	---	---	---
UM-2.0-2.0	0.98	1.25	---	---	---	---	---	---
UM-2.0-1.5	0.99	1.24	---	---	---	---	---	---
UM-2.0-0.8	---	1.07	---	---	---	---	---	---
Mean	1.04	1.16	0.98	0.99	0.99	1.03	1.03	0.94
CoV	0.111	0.134	0.070	0.115	0.129	0.192	0.048	0.050

Table 6 Effect of test orientation on failure pattern of WAAM austenitic stainless steel single shear bolted connections

Specimen group	0°	30°	45°	60°	90°
M-1.0-3.0	SF	---	SF	---	SF
M-1.5-3.0	SF	SF	SF(C)	SF(C)	SF(C)
M-2.0-3.0	CBF	---	CBF	---	CBF
M-2.5-3.0	CBF	---	CBF	---	CBF
M-3.0-3.0	CBF	CBF	CBF	CBF	CBF
M-4.0-3.0	CBF	---	CBF	---	CBF
M-2.0-0.8	NSF(C)	---	NSF(C)	---	NSF(C)
M-2.0-1.5	LTF	LTF	LTF	LTF	LTF
M-2.0-2.0	SF(C)	---	SF(C)	---	SF(C)
UM-1.5-3.0	SF	---	---	---	SF
UM-2.0-2.0	CBF	---	---	---	LTF
UM-2.0-1.5	CBF	---	---	---	LTF
UM-2.0-0.8	NSF	---	---	---	NSF

Figures

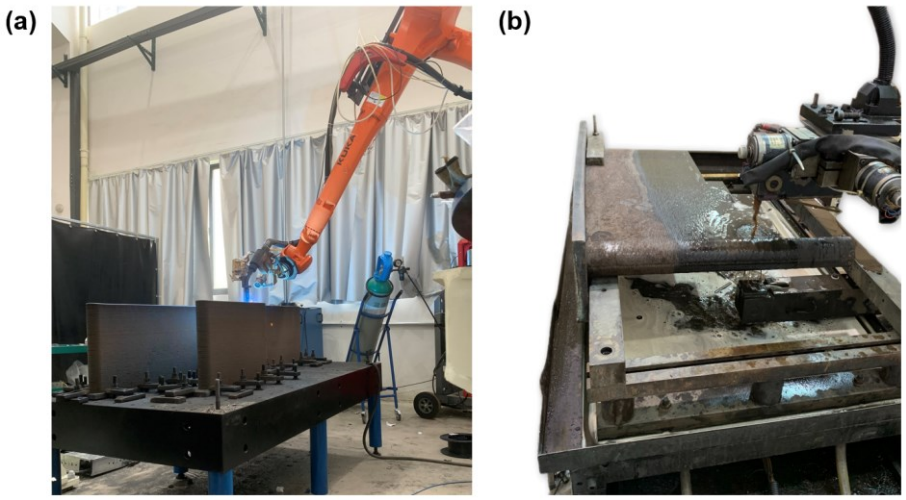

Fig. 1 Fabrication of WAAM specimens: (a). WAAM process; (b). Wire cutting process.

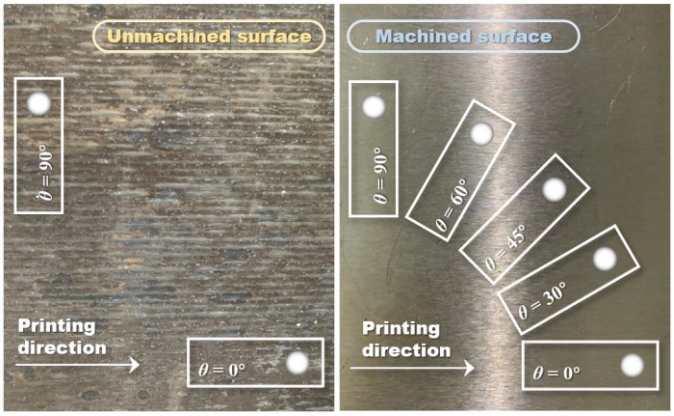

Fig. 2 Orientation convention of specimens related to the printing layer direction.

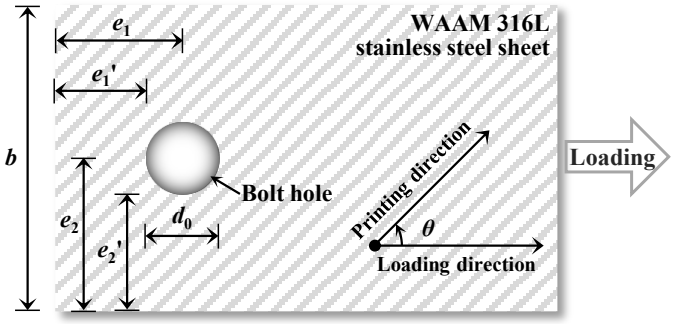

Fig. 3 Definition of nomenclatures

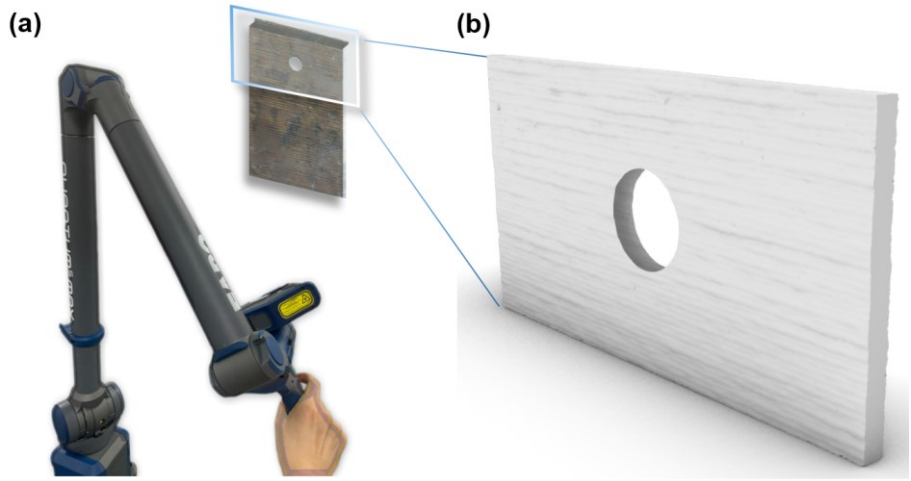

Fig. 4 Geometric measurement: (a). 3D laser scanning; (b). Data processing in Rhino.

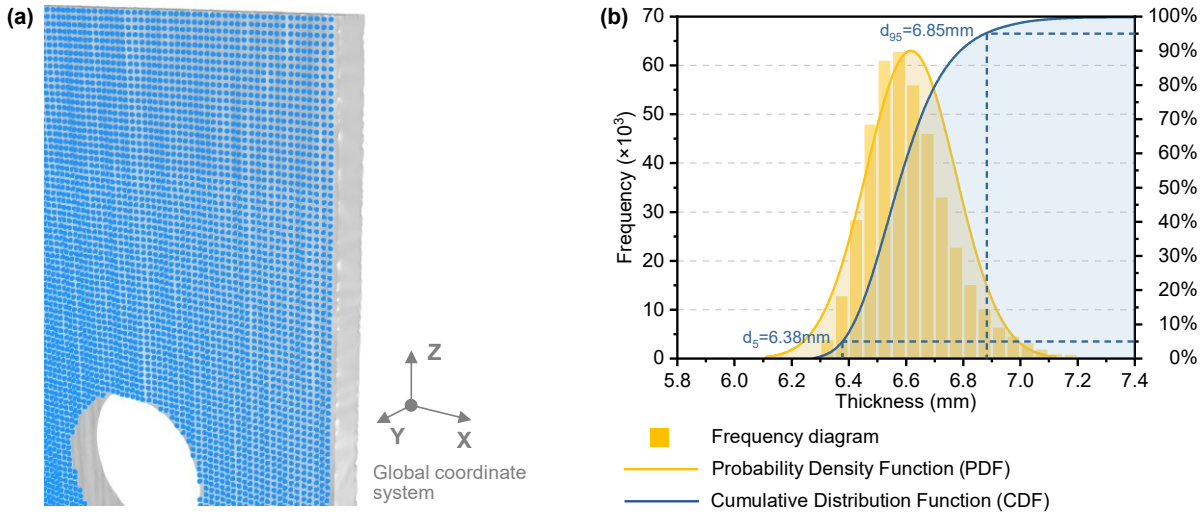

Fig. 5 Geometric analysis for unmachined specimen: (a). Schematic view of cloud point generation for geometric analysis; (b). Thickness distribution of typical unmilled specimen UM-90-1.5-3.0.

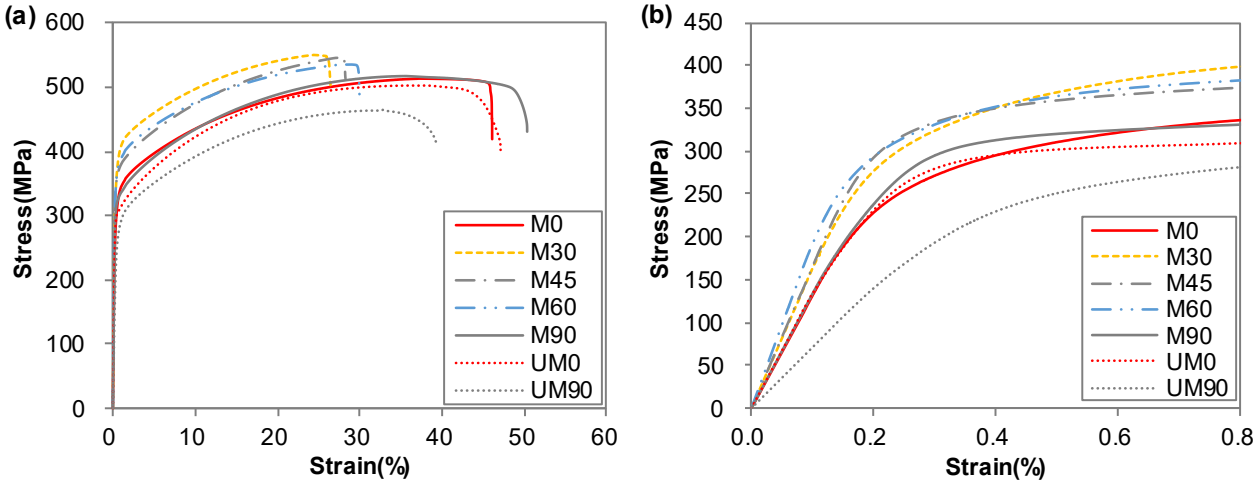

Fig. 6 Stress-strain curves of WAAM 316L austenitic stainless steel specimens with different test orientations: (a). Full range; (b). Initial stage.

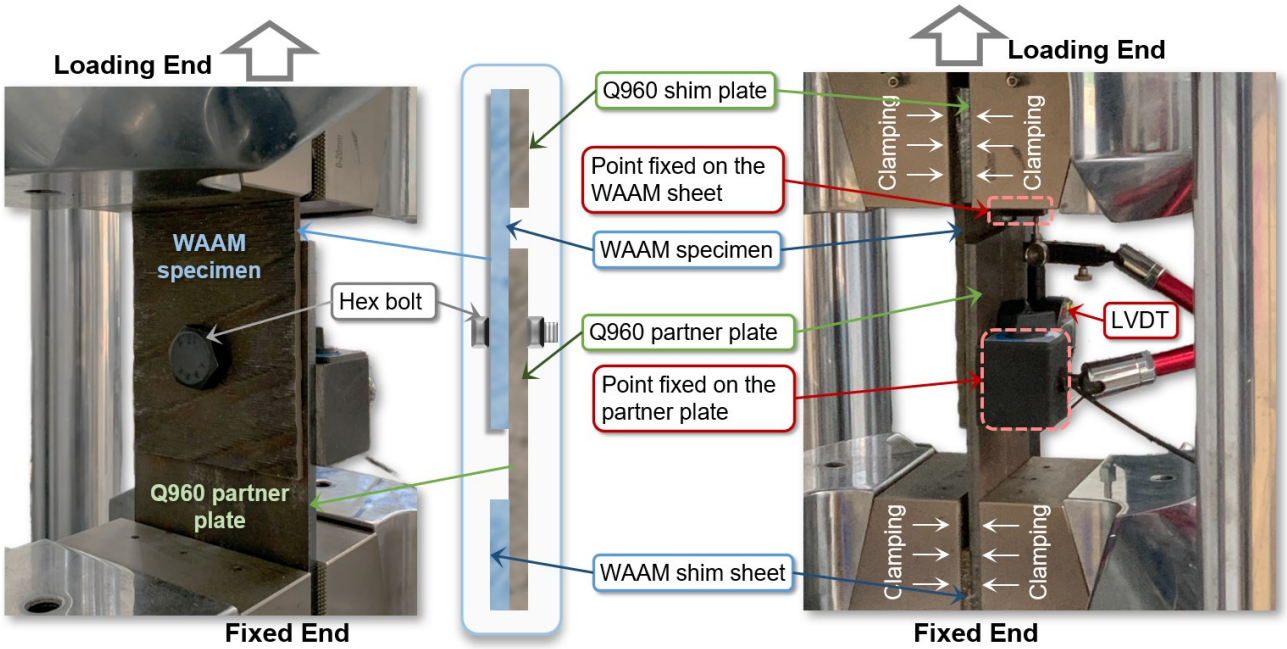

Fig. 7 Single-lap shear test setup

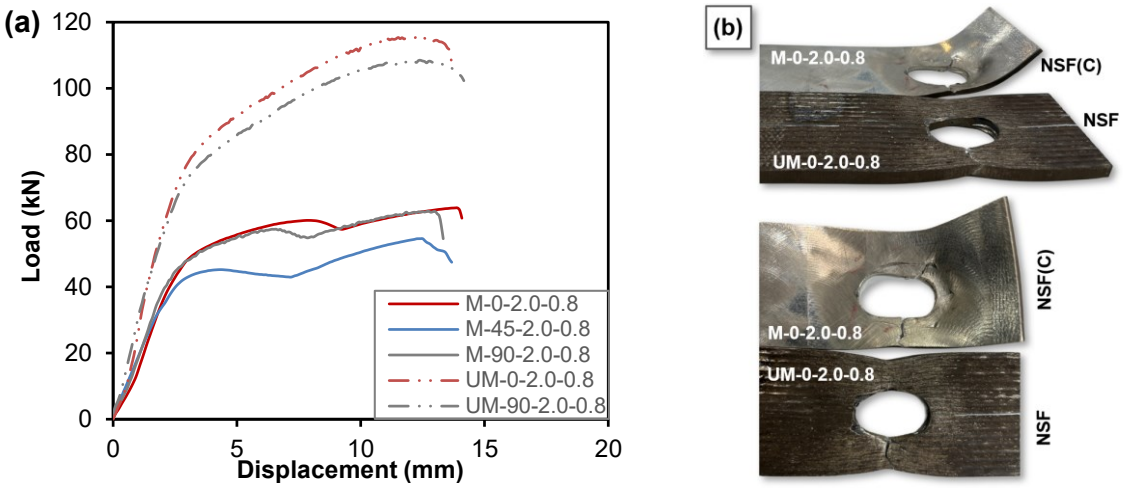

Fig. 8 Net section fracture: (a). Load-displacement curves; (b). Photos of specimens failed in NSF and NSF(C) patterns.

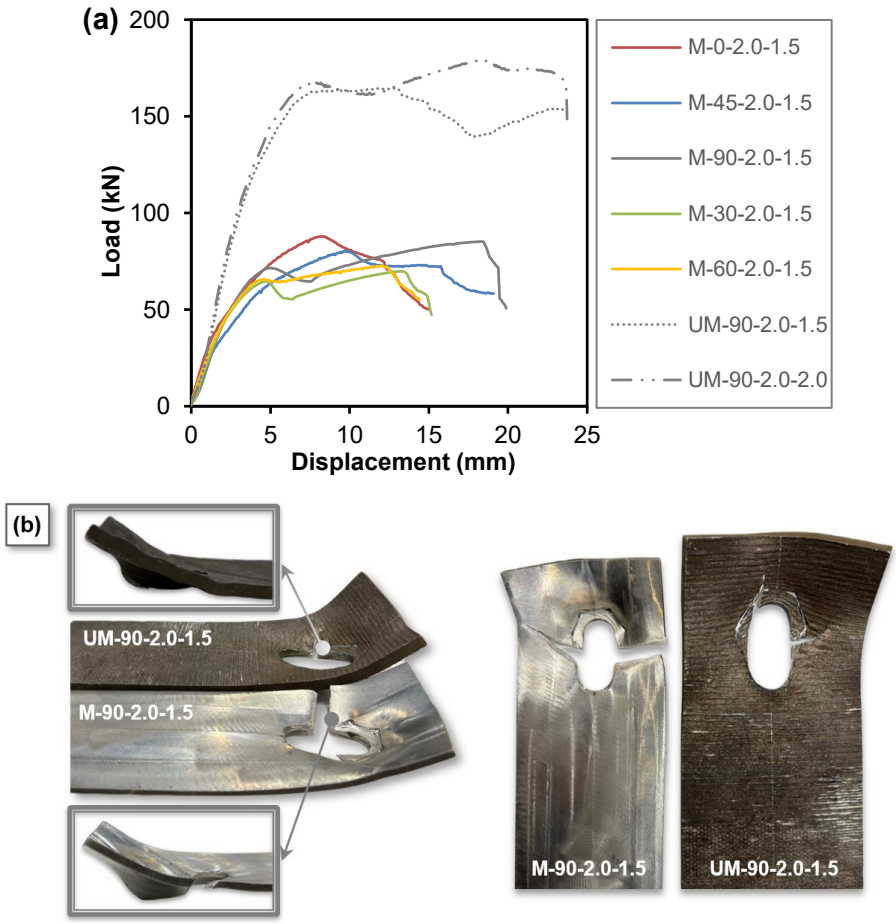

Fig. 9 Localized tearing failure: (a). Load-displacement curves; (b). Photos of specimens failed in LTF pattern.

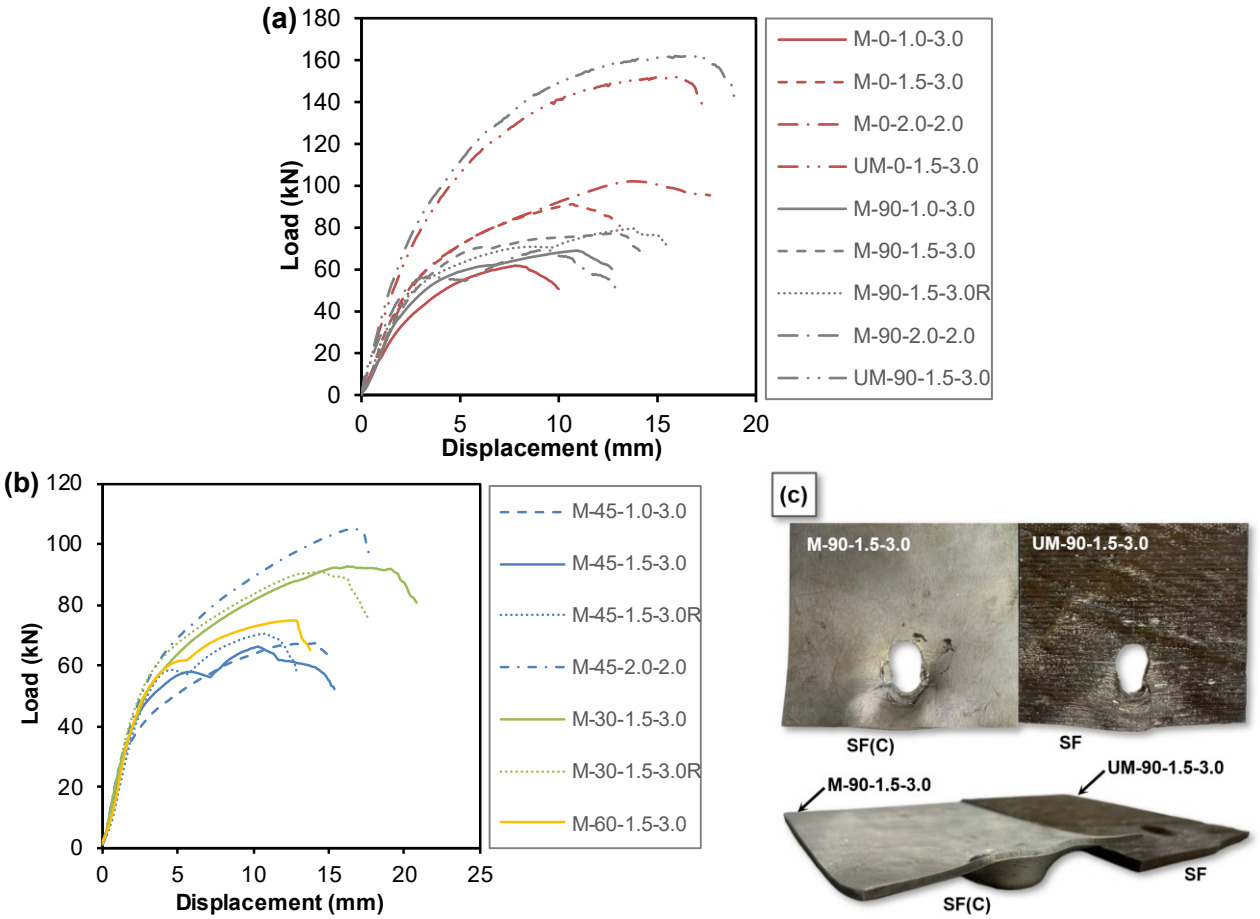

Fig. 10 Shear-out failure: (a). Load-displacement curves of specimens with test orientation of 0° or 90°; (b). Load-displacement curves of machined specimens with test orientation of 30°/45°/60°; (c). Photos of specimens failed in SF and SF(C) patterns.

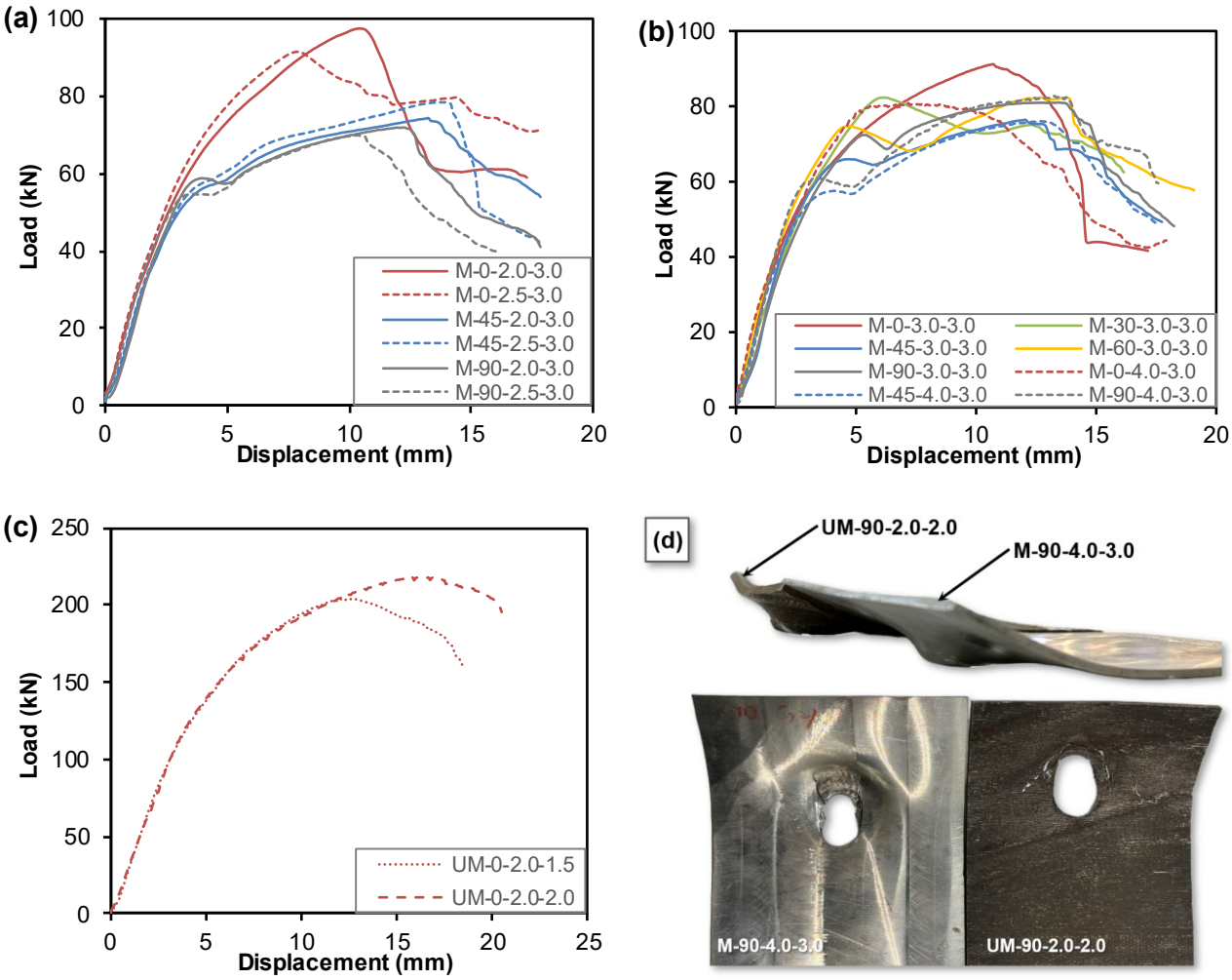

Fig. 11 Curl-bearing failure: (a). load-deformation curves of specimens with $e_1' \leq 2.5d_0$; (b). load-deformation curves of specimens with $e_1' > 2.5d_0$; (c). load-deformation curves of unmachined specimens (d). typical failure photos